Newtonian versus non-Newtonian upper mantle viscosity: Implications for subduction initiation

Magali I. Billen
Department of Geology, University of California, Davis, California, USA

Greg Hirth
Department of Geology and Geophysics, Woods Hole Oceanographic Institution, Woods Hole, Massachusetts, USA

Received 10 May 2005; revised 13 July 2005; accepted 30 August 2005; published 8 October 2005.

[1] The effect of rheology on the evolution of the slab-tip during subduction initiation is analyzed using 2-D numerical flow models. Experimentally determined flow laws have both strong temperature- and stress-dependence, which leads to large local variations in viscosity with direct consequences for subduction initiation. We find that models with Newtonian viscosity lead to flat or coupled subduction due to hydrodynamic stresses that pull the slab-tip up towards the overriding plate. Non-Newtonian rheology reduces these hydrodynamic stresses by decreasing the wedge viscosity and the slab coupling to wedge-corner flow, rendering the small negative-slab buoyancy of the slab-tip sufficient to maintain its dip during the early stages of subduction. **Citation:** Billen, M. I., and G. Hirth (2005), Newtonian versus non-Newtonian upper mantle viscosity: Implications for subduction initiation, *Geophys. Res. Lett.*, *32*, L19304, doi:10.1029/2005GL023457.

1. Introduction

[2] Dynamic coupling of tectonic plates to mantle convection occurs in subduction zones where negative slab buoyancy pulls the plate into the mantle and drives deformation in the surrounding mantle [*Bercovici et al.*, 2000]. While it is recognized that the nature of slab coupling to the mantle depends on the rheology of the slab and the upper mantle [*Gurnis and Hager*, 1988], coupling and deformation of the slab in the upper mantle during subduction initiation has not been widely considered.

[3] Subduction initiation studies have focused on the forces needed to bend or break the lithospheric plate, [*McKenzie*, 1977; *Mueller and Phillips*, 1991; *Fowler*, 1993; *Gurnis et al.*, 2004], exploiting pre-exisiting weaknesses such as fracture zones [*Kemp and Stevenson*, 1996; *Toth and Gurnis*, 1998; *Hall et al.*, 2003] or oceanic-plateau boundaries [*Niu et al.*, 2003], and mechanisms that specifically account for weakening of the lithosphere [*Cloetingh et al.*, 1989; *Regenauer-Lieb et al.*, 2001]. Although, subduction is not self-sustaining until the slab reaches a length of 110–180 km long [*McKenzie*, 1977; *Hall et al.*, 2003], these models have not addressed the balance of hydrodynamic and gravitational forces on the slab-tip as it enters the upper mantle.

[4] Slab dip is controlled by a balance between gravitational forces (negative slab buoyancy), which tend to increase slab dip, hydrodynamic forces (suction) due to induced viscous flow around the slab, which tend to decrease slab dip, and internal deformation of the slab [*Stevenson and Turner*, 1977; *Tovish et al.*, 1978]. For a slab-tip with small negative buoyancy, the hydrodynamic forces can pull up on and viscously couple the slab-tip to the overriding plate. Increasing the slab density by adding compositional buoyancy can overcome the strong hydrodynamic torque [*Kincaid and Sacks*, 1997], but requires compositional density far exceeding expected values [*Ringwood*, 1982].

[5] Laboratory experiments predict that the upper mantle, composed primarily of olivine, deforms by a combination of diffusion (Newtonian) and dislocation (non-Newtonian) creep [*Karato and Wu*, 1993], with the non-Newtonian response dominating in regions of high stress. In addition, localized low viscosity regions can develop in the mantle owing to the presence of water, melt, a reduction of grain-size or the effects non-Newtonian viscosity [*Hirth and Kohlstedt*, 2003]. While some models of subduction initiation have included non-Newtonian viscosity [*Hall et al.*, 2003; *Gurnis et al.*, 2004], they did not explore the role of this choice of rheology on development of the slab-tip.

2. Method

[6] We solve the standard equations of conservation of mass, momentum and energy, for thermal convection without internal heating, in which the mantle is treated as an incompressible fluid and inertial forces are negligible, using the spherical-geometry finite-element code, CitcomT [*Zhong et al.*, 1998]. The model domain, a 2-D slice of a spherical region, and the boundary conditions are shown in Figure 1a. The initial temperature of the plates is calculated assuming a half-space cooling model with a uniform age of 75 Myr (or 25 Myr, model 4 only) for the overriding plate and an age that increases from 0 to 100 Myr across the subducting plate. The plate boundary is modeled as a narrow (20 km), dipping low viscosity shear zone in which the viscosity, $\eta_{sz} = \min(\eta_{eff}, \frac{\sigma_{ysz}}{\dot{\epsilon}})$ is determined from the yield stress σ_{ysz} (see below), $\dot{\epsilon}$ is the second invariant of the strain-rate tensor, and η_{eff} is the effective viscosity (equation (1)) (Figure 1b).

[7] A visco-plastic rheology is used for the mantle and lithosphere. The plastic response is applied to cold regions ($T \leq 800°C$) and to the shear zone as a yield stress, σ_y =

0094-8276/05/2005GL023457$05.00

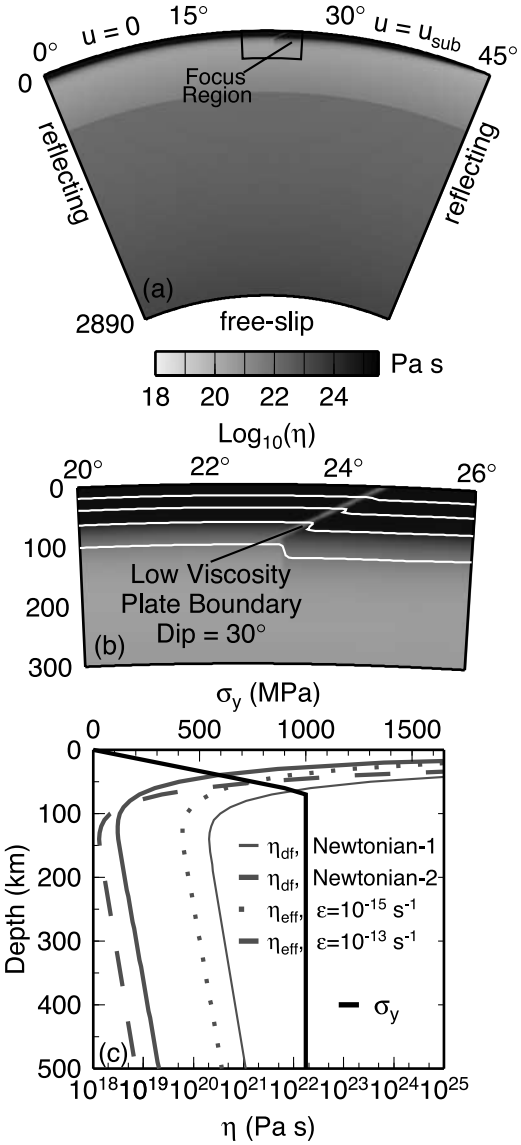

Figure 1. Model setup. (a) Full model domain with boundary conditions (0–25° – overriding plate, $u = 0$; 25–45° – subducting plate, $u = u_{sub}$) and initial viscosity structure (Newtonian-1). Top and bottom boundaries are isothermal. Element size varies from 1.5 × 2.5 km in the top-center, to 16.5 × 10 km in the bottom-edges of the model domain. (b) Enlarged view of subduction zone region with the shear zone plate boundary and temperature contours (300°C). (c) Depth profiles of viscosity and yield stress. See color version of this figure in the HTML.

$\min(\sigma_{max}, \sigma_0 + \sigma'_y z)$, where σ_{max} = 1000 MPa approximates the behavior of low-temperature plasticity [*Goetze and Evans*, 1979], σ_0 = 0.1 MPa is the rock strength in the upper kilometer and σ'_y = 15 MPa/km is the stress gradient in the lithosphere assuming approximately hydrostatic pore fluid pressure (pore fluid ratio, λ = 0.9) and a coefficient of friction, μ = 0.6 [*Kohlstedt et al.*, 1995] (Figure 1c). In the shear zone, σ'_{ysz} = 0.176 MPa/km for μ = 0.4 and λ = 0.99, which gives a maximum shear zone yield stress of 17.5 MPa at 100 km depth. The effective viscosity

$$\eta_{eff} = \frac{\eta_{df}\eta_{ds}}{\eta_{df} + \eta_{ds}} \quad (1)$$

accounts for deformation in which the total strain-rate is accommodated by diffusion creep, η_{df}, and dislocation creep, η_{ds}. The transition from diffusion- to dislocation-dominated creep is characterized by the transition strain-rate, the strain-rate at which $\eta_{df} = \eta_{ds}$ ($\dot{\epsilon}_{tran} = 10^{-15}$ s^{-1} at 250 km depth for the parameters used in this study). The viscosity law when no melt is present and water content is constant is given by

$$\eta = \left(\frac{d^p}{AC_{OH}^r}\right)^{\frac{1}{n}} \dot{\epsilon}^{\frac{1-n}{n}} \exp\left[\frac{E^* + PV^*}{RT}\right] \quad (2)$$

where A is the experimentally determined pre-exponential factor, d is the grain size, C_{OH} is the concentration of hydroxyl ions in the olivine, E^* is the activation energy, V^* is the activation volume and P is the lithostatic pressure.

[8] The viscosity parameters are taken from *Hirth and Kohlstedt* [2003, Table 1] for wet diffusion creep ($A = 10^6$, $n = 1$, $p = 3$, $r = 1$, $E^* = 335$ kJ, $V^* = 4 \times 10^{-6}$ m^3/mol) and wet dislocation creep ($A = 90$, $n = 3.5$, $p = 0$, $r = 1.2$, $E^* = 480$ kJ, $V^* = 11 \times 10^{-6}$ m^3/mol) for olivine at constant C_{OH}. The absolute value of the viscosity is determined by choice of the water content and grain-size. The viscosity profile (Newtonian-1, Effective) uses C_{OH} = 300 H/10^{6}Si and d = 10 mm throughout the upper mantle and lithosphere, which gives an effective viscosity of 1×10^{20} Pa-s at a depth of 250 km for both the diffusion and dislocation creep laws at the transition strain-rate (Figure 1c). These values are modified to C_{OH} = 3000 H/10^{6}Si and d = 4 mm in the upper mantle for a subset of Newtonian viscosity models (Newtonian-2) to give a viscosity similar to that which occurs in the effective viscosity models as a result of strain-rates that exceed the transition strain-rate.

[9] The incorporation of a yield stress in the models leads to a plastic response everywhere within the cold interior of the slab. Given the strength profile for the lithosphere with a visco-elastic-plastic rheology [*Goetze and Evans*, 1979], deformation of the slab is accommodated by both elastic and viscous strain until the applied stress exceeds the yield

Table 1. Model Parameters[a]

Model	Rheology	u_{sub}	θ_{sz}	Sub.-Style
1	Newt-1	2.5	30°	coupled
2	Newt-1	5.0	30°	coupled
3	Newt-1	7.5	30°	coupled/flat
4[b]	Newt-1	5.0	30°	flat
5[c]	Newt-1	5.0	30°	flat
6	Newt-1	5.0	45°	coupled/flat
7	Newt-1	5.0	60°	coupled/flat
8	Eff.	2.5	30°	normal
9	Eff.	5.0	30°	normal
10	Eff.	7.5	30°	normal
11	Newt-2	2.5	30°	coupled
12	Newt-2	5.0	30°	coupled/flat

[a]Subduction velocity in cm/yr. θ_{sz} is the shear zone dip.
[b]The overriding plate age is 75 Myr for all models except model 4 with an age of 25 Myr.
[c]Model 5 is Newtonian with no yield stress.

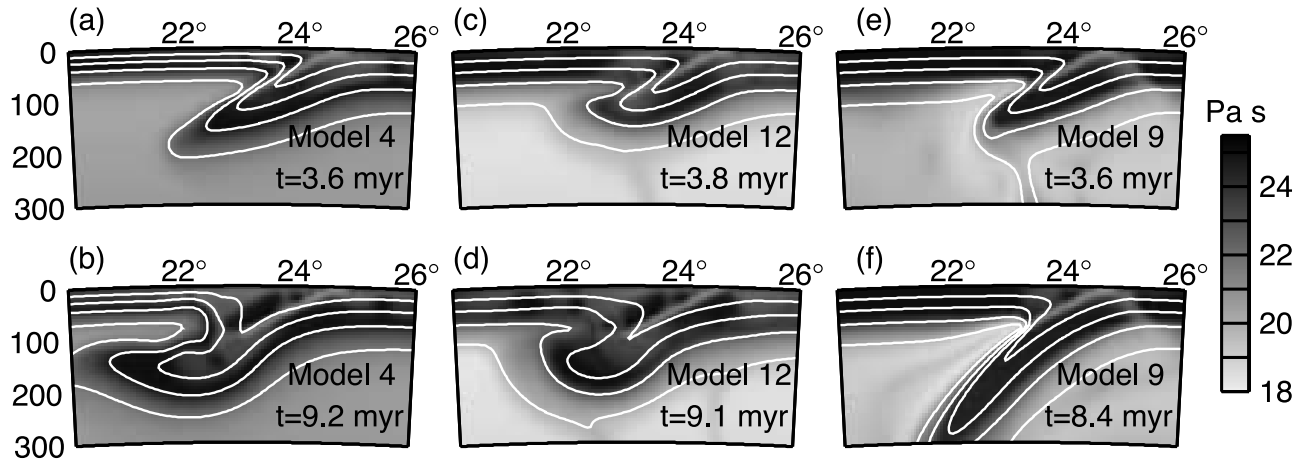

Figure 2. Model results. Viscosity ($\log_{10}(\eta)$) overlain by temperature contours (300°C) for (a)–(b) Model 4–flat, (c)–(d) Model 12–coupled and (e)–(f) Model 9–normal. See color version of this figure in the HTML.

stress. In our models, although we do not explicitly include elasticity, once the yield stress is exceeded the stresses acting on the slab would be large enough to overcome both the visco-plastic and elastic resistance to deformation.

3. Results

[10] The effect of Newtonian versus non-Newtonian viscosity on the deformation of the slab-tip during subduction initiation is analyzed for a series of models in which either effective viscosity or a Newtonian viscosity is used and the imposed subduction velocity, shear zone dip, age of the overriding plate and/or yield stress are varied. A subset of these model results are summarized in Table 1 with three models illustrating the range of behavior shown in Figure 2.

[11] Three styles of subduction of the slab-tip were observed in the models: normal, coupled and flat. Normal subduction is characterized by subduction that maintains a distinct low viscosity and high temperature boundary between the slab and overriding plate. Coupled subduction occurs when overall thickening of the subducting slab causes it to viscously couple to and partially entrain the lower portion of the overriding plate. Flat subduction occurs when a distinct decrease in slab dip causes the slab-tip to flatten beneath the overriding plate. In some models initially coupled subduction leads to formation of a flat slab (labeled coupled/flat in Table 1), while all flat slabs become viscously coupled to the overriding plate.

[12] All of the Newtonian viscosity models resulted in flat, coupled or coupled/flat subduction regardless of other rheology parameters (Newt-1 and Newt-2), subduction rate (2.5–7.5 cm/yr), shear zone dip (30°, 45°, and 60°), age of the overriding plate (25 and 75 myr) and yield stress (depth-dependent or no yield stress). These models start with a distinct separation of the slab and overriding plate, however as the wedge corner cools, the viscosity increases. The hydrodynamic stress acting on the surface of the slab-tip is proportional to both the viscosity and the magnitude of velocity in the mantle above the slab [*Tovish et al.*, 1978]. The temperature dependence of the flow laws leads to a sharp increase in viscosity with temperature in the wedge corner (Model 4, Figure 2a). Therefore the hydrodynamic stress increases rapidly as the viscosity increases even as the flow velocity above the slab decreases. Because the slab can deform and its buoyancy is small, the increase in hydrodynamic stress thickens and flattens the slab against the overriding plate (Figure 2b). In Newtonian models with a lower asthenospheric viscosity (Newt-2: $\sim$10 $\times$ smaller), a distinct separation of the slab and overriding plate persists for slightly longer times, but the slab also eventually becomes coupled to the overriding plate (Model 12, Figures 2c and 2d).

[13] During subduction initiation the wedge corner is subject to high stresses as the slab-tip is pushed into the mantle and a constricted corner flow develops above the slab. In the effective viscosity models these stresses act to decrease the wedge-corner viscosity due to the non-Newtonian component of the effective viscosity. In addition, the decrease in viscosity surrounding the slab partially decouples the slab from the surrounding mantle creating a sharper gradient in velocity above the slab and a lower mantle flow velocity in the wedge away from the slab. Both these effects act to decrease the hydrodynamic stresses on the slab. As soon as the slab-tip pushes beneath the overriding plate a weak zone develops above the slab-tip, even as this region cools (Model 9, Figures 2e and 2f). This weak zone is maintained as subduction continues allowing advection of the mantle into the narrow wedge corner and thus maintaining warmer wedge-corner temperatures.

4. Discussion and Conclusions

[14] The minimum convergence velocity needed to overcome thermal equilibration during subduction initiation is estimated as 1.0–1.5 cm/yr [*McKenzie*, 1977; *Hall et al.*, 2003], while the upper limit depends on the relative speed of the converging plates across the plate boundary. A convergence velocity of 1.0–2.0 cm/yr provides sufficient driving force to initiate subduction in models with a young (<10 Myr) overriding plate and purely non-Newtonian viscosity for the mantle [*Hall et al.*, 2003]. For the viscosity parameters used in our study a slow convergence rate of 2.5 cm/yr is sufficient to maintain separation between the slab and overriding plate during subduction initiation. However, this result depends on the grain size and water content, which determines the transition strain-rate, and thus the

strain-rate needed to overcome the affects of thermal cooling and temperature-dependence of viscosity in the wedge corner. For example, a smaller grain-size would decrease the diffusion creep component of the effective viscosity, but would increase the transition strain-rate, thus diminishing the strain-rate weakening response. Dehydration of the slab-tip and hydration of the wedge corner or dynamic recrystallization leading to an even larger reduction in grain size could further decrease the wedge-corner viscosity, although the behavior of models 11 and 12 indicate that these effects may not be sufficient in the absence of dislocation creep.

[15] We have shown that an effective viscosity with a non-Newtonian component facilitates subduction initiation by decreasing the hydrodynamic stresses and internal deformation of the slab. Although some aspects of convection (e.g. overall heat transport) with non-Newtonian viscosity can be simulated using a Newtonian viscosity with a reduced activation energy [*Christensen*, 1983], non-Newtonian viscosity with the full temperature-dependence creates strong local variations in viscosity that lead to considerably different dynamics.

[16] **Acknowledgments.** M. I. Billen thanks Woods Hole Oceanographic Institution and the USGS for support as a post-doctoral fellow. We also thank two anonymous reviewers for their comments and suggestions.

References

Bercovici, D., Y. Ricard, and M. Richards (2000), The relation between mantle dynamics and plate tectonics: A primer, in *The History and Dynamics of Global Plate Motions*, *Geophys. Monogr. Ser.*, vol. 21, edited by M. A. Richards, R. Gordon, and R. V. der Hilst, pp. 5–46, AGU, Washington, D. C.

Christensen, U. R. (1983), Convection in a variable-viscosity fluid: Newtonian versus power-law rheology, *Earth Planet. Sci. Lett.*, *64*, 153–162.

Cloetingh, S., R. Wortel, and N. J. Vlaar (1989), On the initiation of subduction zones, *Pure Appl. Geophys.*, *129*, 7–25.

Fowler, A. C. (1993), Boundary layer theory of subduction, *J. Geophys. Res.*, *98*, 21,997–22,005.

Goetze, C., and B. Evans (1979), Stress and temperature in the bending lithosphere as constrained by experimental rock mechanics, *Geophys. J. R. Astron. Soc.*, *59*, 463–478.

Gurnis, M., and B. H. Hager (1988), Controls of the structure of subducted slabs, *Nature*, *335*, 317–321.

Gurnis, M., C. Hall, and L. Lavier (2004), Evolving force balance during incipient subduction, *Geochem. Geophys. Geosyst.*, *5*, Q07001, doi:10.1029/2003GC000681.

Hall, C. E., M. Gurnis, M. Sdrolias, L. Lavier, and R. D. Müller (2003), Catastrophic initiation of subduction following forced convergence across fracture zones, *Earth Planet. Sci. Lett.*, *212*, 15–30.

Hirth, G., and D. Kohlstedt (2003), Rheology of the upper mantle and the mantle wedge: A view from the experimentalists, in *Inside the Subduction Factory*, *Geophys. Monogr. Ser.*, vol. 138, edited by J. Eiler, pp. 83–105, AGU, Washington, D. C.

Karato, S., and P. Wu (1993), Rheology of the upper mantle: A synthesis, *Science*, *260*, 771–778.

Kemp, D. V., and D. J. Stevenson (1996), A tensile, flexural model of the initiation of subduction, *Geophys. J. Int.*, *125*, 73–94.

Kincaid, C., and I. S. Sacks (1997), Thermal and dynamical evolution of the upper mantle in subduction zones, *J. Geophys. Res.*, *102*, 12,295–12,315.

Kohlstedt, D. L., B. Evans, and S. J. Mackwell (1995), Strength of the lithosphere: Constraints imposed by laboratory experiments, *J. Geophys. Res.*, *100*, 17,587–17,602.

McKenzie, D. P. (1977), The initiation of trenches: A finite amplitude instability, in *Island Arcs, Deep Sea Trenches and Back-Arc Basins*, *Maurice Ewing Ser.*, vol. 1, edited by M. Talwani and W. C. Pitman III, pp. 57–62, AGU, Washington, D. C.

Mueller, S., and R. J. Phillips (1991), On the initiation of subduction, *J. Geophys. Res.*, *96*, 651–665.

Niu, Y., M. J. O'Hara, and J. A. Pearce (2003), Initiation of subduction zones as a consequence of lateral compositional buoyancy contract within the lithosphere: A petrological perspective, *J. Petrol.*, *44*, 851–866.

Regenauer-Lieb, K., D. A. Yuen, and J. Branlund (2001), The initiation of subduction: Criticality by addition of water, *Science*, *294*, 578–580.

Ringwood, A. E. (1982), Phase transformations and differentiation in subducted lithosphere: Implications for mantle dynamics, basalt petrogenesis, and crustal evolution, *J. Geol.*, *90*, 611–643.

Stevenson, D. J., and J. S. Turner (1977), Angle of subduction, *Nature*, *270*, 334–336.

Toth, J., and M. Gurnis (1998), Dynamics of subduction initiation at preexisting fault zones, *J. of Geophys. Res.*, *103*, 18,053–18,067.

Tovish, A., G. Schubert, and B. P. Luyendyk (1978), Mantle flow pressure and the angle of subduction: Non-Newtonian corner flows, *J. Geophys. Res.*, *83*, 5892–5898.

Zhong, S., M. Gurnis, and L. Moresi (1998), Role of faults, nonlinear rheology, and viscosity structure in generating plates from instantaneous mantle flow models, *J. Geophys. Res.*, *103*, 15,255–15,268.

M. I. Billen, Department of Geology, University of California, Davis, Davis, CA 95616, USA. (billen@geology.ucdavis.edu)

G. Hirth, Department of Geology and Geophysics, Woods Hole Oceanographic Institution, Woods Hole, MA 02543, USA. (ghirth@whoi.edu)